



Numerical approximation of the dissipativity of energy and spectrum for a damped Euler-Bernoulli beam with variable coefficients



Bomisso Gossrin Jean-Marc^{a,*}, Yapi Serge Alain Joresse^a, Touré Kidjégbo Augustin^b

^aUniversité Nangui Abrogoua d'Abobo-Adjamé and UFR Sciences Fondamentales et Appliquées, Côte d'Ivoire.

^bInstitut National Polytechnique Houphouët-Boigny de Yamoussoukro, Côte d'Ivoire.

Abstract

This article concerns the numerical study of the behaviour of a flexible beam of Euler-Bernoulli to which one adds to its internal composition a damping of the viscous type. This damping naturally exerts a dissipative force (or viscous damping force) on the beam and opposes any deformation, in proportion to the rate of deformation. We are therefore interested in the impact of the damper on the exponential stability of the beam. We develop here a numerical method which faithfully reproduces the theoretical results obtained by several authors. Simulations are provided to illustrate our results.

Keywords: Beam equation, viscous damping, Galerkin approximation, finite elements, error estimates.

2020 MSC: 35A15, 35B35, 35B45, 37N30, 35L20, 65N30, 74S05.

©2023 All rights reserved.

1. Introduction and statement of the problem

The objective of this paper is to develop a stable and convergent numerical method for a damped Euler-Bernoulli beam with variable coefficients that confirms the theoretical results obtained in [17]. The following Euler-Bernoulli beam with indefinite viscous damping is the issue that we will take into consideration:

$$m(x)y_{tt}(x, t) + (EI(x)y_{xx}(x, t))_{xx} + \gamma(x)y_t(x, t) = 0, x \in (0, 1), t > 0, \quad (1.1)$$

with the initial conditions

$$y(x, 0) = y_0(x), \quad y_t(x, 0) = y_1(x), \quad (1.2)$$

and the boundary conditions

$$EI(0)y_{xx}(0, t) = 0, \quad t > 0, \quad -EI(1)y_{xx}(1, t) = 0, \quad t > 0, \quad (1.3)$$

where t stands for the time and x for the spatial position. The length of the beam is chosen to be unity. The physical meanings of the various mathematical quantities are shown below:

*Corresponding author

Email addresses: bogojm@yahoo.fr (Bomisso Gossrin Jean-Marc), sergeyapi965@gmail.com (Yapi Serge Alain Joresse), latoureci@gmail.com (Touré Kidjégbo Augustin)

doi: [10.22436/jnsa.016.03.01](https://doi.org/10.22436/jnsa.016.03.01)

Received: 2023-04-20 Revised: 2023-06-26 Accepted: 2023-07-28

- $m(x)$ is the mass density;
- $EI(x)$ is the stiffness of the beam;
- $y(x, t)$ denotes the transverse displacement.

In what follows, we shall always assume that:

$$m(x), EI(x) \in C^4[0, 1]; \quad m(x), EI(x) > 0.$$

Moreover, the viscous coefficient γ is a continuous function and nonnegative that is assumed to satisfy the condition (see [17])

$$\int_0^1 \left(\frac{\gamma(x)}{m(x)} \right) \left(\frac{m(x)}{EI(x)} \right)^{1/4} dx > 0. \quad (1.4)$$

Notice that the condition (1.4) will allow γ to be indefinite in the interval $[0, 1]$. The total energy associated to the above system is (see e.g. [11, 13] and reference therein)

$$\mathbb{E}(t) = \frac{1}{2} \int_0^1 EI y_{xx}^2 dx + \frac{1}{2} \int_0^1 m y_t^2 dx.$$

After a straightforward calculation, we have

$$\frac{d}{dt} \mathbb{E}(t) = - \int_0^1 \gamma |y_t|^2 dx \leq 0. \quad (1.5)$$

The expression (1.5) shows that the energy $\mathbb{E}(t)$ is non-increasing. Then the system is dissipative.

The following describes the range of work involved in investigating the model shown in equation (1.1)-(1.3). The study of the exponential stability of Euler-Bernoulli problems has interested several authors. Let us note that for a given system, the exponential stability is the most sought after because it offers the convergence with the guarantee of a good order of convergence. Others have looked at the case where the system would include a damping or viscous friction term with variable coefficients modelled by a function noted $\gamma(\cdot)$. In [3], a damped Euler-Bernoulli beam with variable coefficients clamped at one end and subjected to a force control in rotation and velocity rotation was considered. The undamped case had already been researched in [2]. Under certain conditions, it was proved that the system is exponentially stable. The question arose to know is that the fact of adding a damping to the first problem allows to have an exponential stability? The answer to this question is yes. To show the exponential stability damping system, they prove that the system operator has Riesz basis property, by setting conditions on the parameters α and β . Following [15], a flexible beam with nonuniform thickness or density, that is clamped at one end, submitted to a linear boundary control force in position and velocity at the free end has been studied. A question similar to the previous one was asked in order to know the values for which the damping system reached the exponential stability? Thanks to a theorem the condition on the value was found. In order not to have to repeat ourselves, our problem [17] was the subject of an exponential stability study. For these three articles mentioned no numerical study has been made for the moment concerning one of them to our knowledge. We are interested in the numerical study of the problem (1.1)-(1.3).

Several books have discussed the numerical analysis of Euler-Bernoulli beams in literature, and there are various ways. It is well known that in literature (see for instance [8, 10]) to geometrically describe the spectrum of an operator, the way used is the following: the authors use the finite differences method [6, 12] and apply QZ method [7, 9]. At this level, we proceed differently. We rely instead on the Hermite finite element method which is not as easy because of the numerous calculations to be performed in order to determine the approximations of the mass, stiffness, and damping matrices.

In Section 2, we present the main results concerning the numerical study. We rely on the weak formulation of the problem to develop a numerical method. The discretization of this system is done in two steps: for the discretization in space, we use the finite element method, and the Crank-Nicolson method for the discretization in time in order to have the complete discretization. The main results on the convergence of the numerical schemes are given in Theorems 2.4 and 2.9. The numerical method is validated by various simulation examples, and the convergence is demonstrated in the Section 3. We are interested in the implementation of the coefficients both in the constant and in the variable case.

2. Main results

2.1. State space, operator \mathcal{A} , and some basic properties

This section of research is devoted to basic results, theorems, and definition. These will be very useful for the continuation especially for the theorem concerning the stability. We will have to make sure that this property is verified in the numerical simulations. We transform system (1.1)-(1.3) into an abstract evolution equation on an appropriately constructed Hilbert space.

We define a Hilbert space by

$$\mathbb{H} = \mathbb{V} \times L^2(0, 1)$$

with an inner product norm in \mathbb{H} as

$$\|(f, g)\|_{\mathbb{H}}^2 := \int_0^1 EI(x)|f''(x)|^2 dx + \int_0^1 m(x)|g(x)|^2 dx, \quad \forall f, g \in \mathbb{H},$$

and

$$\mathbb{V} = H_E^2(0, 1) = \{y \in H^2(0, 1), y(0) = y(1) = 0\}$$

and define a linear operator \mathcal{A} by

$$D(\mathcal{A}) = \{(f, g)^T \in \mathbb{H} | f \in H^4(0, 1) \cap \mathbb{V}, g \in \mathbb{V}, f''(0) = 0, f''(1) = 0\}$$

and

$$\mathcal{A}(f, g) := \left(g, -\frac{1}{m(x)} ((EI(x)f''(x))'' + \gamma(x))g \right).$$

Under these notations, system (1.1)-(1.3) can be formulated into an abstract evolution equation in \mathbb{H} :

$$\begin{cases} \frac{d}{dt}w(t) = \mathcal{A}w(t), \\ w(0) = w_0 \in \mathcal{H}, \end{cases} \tag{2.1}$$

where $w(t) = (y(x, t), y_t(x, t))$. The first result we obtain with this formulation for \mathcal{A} is the following.

Theorem 2.1. *The operator \mathcal{A} defined as before generates a C_0 -semigroup of contractions on \mathbb{H} , denoted by $\{T(t)\}_{t \geq 0}$. Furthermore, \mathcal{A} is invertible with \mathcal{A}^{-1} being compact.*

Proof. Let \mathcal{A}_0 and \mathcal{A} be the operators respectively obtained of problem (1.1)-(1.3) for undamped and damped cases. In the Theorem 2.1 of [17], \mathcal{A}_0 is a skew-adjoint operator and generates a C_0 -semi-group on \mathbb{V} , and hence \mathcal{A} generates a C_0 -semi-group $e^{\mathcal{A}t}$ on \mathbb{V} . Furthermore, in the proof of Theorem 2.2 of [17], the authors have proved that \mathcal{A}^{-1} is compact on \mathbb{V} by showing that for any $G := (g_1, g_2) \in \mathbb{V}$, there exists a unique $F := (f_1, f_2) \in D(\mathcal{A})$ such that $\mathcal{A}F = G$. □

Thus, from Theorem 2.1, we get the theorem of stability.

Theorem 2.2. *Assume that $w(t)$ is the mild solution of (2.1) for some $w_0 \in \mathbb{H}$. Then $w(t) \rightarrow 0$ in \mathbb{H} , when $t \rightarrow \infty$.*

2.2. Weak formulation

Now, multiplying equation (1.1) by $\phi \in \mathbb{V}$ and integrating over $(0, 1)$, we have:

$$\int_0^1 m u_{tt} \phi \, dx + \int_0^1 (EI u_{xx})_{xx} \phi \, dx + \int_0^1 \gamma(x) u_t \phi \, dx = 0, \forall \phi \in \mathbb{V}, t > 0.$$

Integrating twice by parts and taking into account the boundary conditions it follows:

$$\int_0^1 m u_{tt} \phi \, dx + \int_0^1 EI u_{xx} \phi_{xx} \, dx + \int_0^1 \gamma u_t \phi \, dx = 0, \forall \phi \in \mathbb{V}, t > 0.$$

In order to give the definition of the weak solution of our problem, we rely on the work of Banks [1], which leads us to consider two Hilbert spaces. These are $\mathbb{X} = \mathbb{R}^2 \times L^2(0, 1)$ with the inner product

$$\langle \zeta, \psi \rangle_{\mathbb{X}} = \zeta_1 \psi_1 + \zeta_2 \psi_2 + \langle m \zeta_3, \psi_3 \rangle_{L^2(0,1)}$$

for all $\zeta = (\zeta_1, \zeta_2, \zeta_3)$, $\psi = (\psi_1, \psi_2, \psi_3) \in \mathbb{X}$; and $\mathbb{Y} = \mathbb{R}^2 \times H^2_{\Gamma}(0, 1) = \{\hat{y} = (y(1), y_x(1), y); y \in \mathbb{V}\}$ with the inner product

$$\langle \hat{y}_1, \hat{y}_2 \rangle_{\mathbb{Y}} = \langle (y_1)_{xx}, (y_2)_{xx} \rangle_{L^2(0,1)}.$$

\mathbb{Y} is densely embedded in \mathbb{X} . Then the dual of \mathbb{X} is densely embedded in the dual of \mathbb{Y} . If we choose to identify \mathbb{X} with its dual \mathbb{Y}' we have

$$\mathbb{Y} \subset \mathbb{X} \equiv \mathbb{X}' \subset \mathbb{Y}'.$$

Then we consider two bilinear forms a_1 and a_2 defined by:

$$a_1 : \mathbb{Y} \times \mathbb{Y} \longrightarrow \mathbb{R} \quad (\hat{y}_1, \hat{y}_2) \mapsto a_1(\hat{y}_1, \hat{y}_2) = \langle EI \hat{y}_1, \hat{y}_2 \rangle_{\mathbb{Y}}$$

and

$$a_2 : \mathbb{X} \times \mathbb{X} \longrightarrow \mathbb{R} \quad (\zeta, \psi) \mapsto a_2(\zeta, \psi) = \langle \gamma \zeta_3, \psi_3 \rangle_{L^2(0,1)}.$$

A definition of a weak solution can now be provided.

Definition 2.3. Let $T > 0$ be fixed. We say that $\hat{y} = (y(1), y_x(1), y)$ is a weak solution of problem (1.1)–(1.3) on $(0, 1)$ if

$$\hat{y} \in L^2(0, T; \mathbb{Y}) \cap H^1(0, T; \mathbb{X}) \cap H^2(0, T; \mathbb{Y}')$$

and satisfies

$$\langle \hat{y}_{tt}, \hat{\phi} \rangle_{\mathbb{Y}, \mathbb{Y}'} + a_1(\hat{y}, \hat{\phi}) + a_2(\hat{y}_t, \hat{\phi}) = 0 \tag{2.2}$$

for almost everywhere $t \in (0, T)$ and for all $\hat{\phi} \in \mathbb{Y}$ with the following initial conditions:

$$\hat{y}(0) = \hat{y}_0 = (y_0(1), (y_0)_x(1), y_0) \in \mathbb{Y}, \quad \hat{y}_t(0) = \hat{z}_0 = (z_0(1), (z_0)_x(1), z_0) \in \mathbb{X}.$$

We admit the existence and uniqueness of the weak solution.

2.3. The Semi-discrete Approximation by FEM

In this subsection, we will approximate the original problem (1.1)–(1.3) with FEM method. Since that (1.1) involves the spatial derivative of four orders, $H^2(0, 1)$ should possess the conforming FEM space.

2.3.1. Piecewise cubic Hermite polynomials

We assume that the Euler-Bernoulli beam is the segment $[0, 1]$. We divide the interval $[0, 1]$ into a finite number of subintervals $I_i = [x_i, x_{i+1}]$, $i = 0, 1, \dots, n - 1$, using the grid points:

$$0 < x_0 < x_1 < \dots < x_n = 1,$$

where I_i is called element and set $h = x_{i+1} - x_i$ the size of this element. We define a finite-dimensional

space as follows:

$$V^h = \{y_h \in C^1[0, 1] | y_h \in P_3(I_i) \forall i = 0, 1, \dots, N, y_h(0) = y_h(1) = y_h'(0) = y_h'(1)\},$$

where $P_3(I_i)$ is the space of all polynomials of degree less than or equal to 3 over the subinterval I_i . Obviously, we have $V^h \in \mathbb{V}$. Thus, we can write

$$V^h = \text{span}\{\phi_1, \phi_2, \dots, \phi_{2n}\},$$

where we use the finite element method with cubic Hermite polynomials $\psi_{i,j}$ ($j = 1, \dots, 4$) as functions reference from which we build polynomials ϕ_i ($i = 1, \dots, N$) (see [16]). With the separation of variables, the approximate solution $y_h \in V^h$, which we seek can be written as follows:

$$y_h(x, t) = \sum_{j=0}^n [y_j(t)\phi_{2j-1}(x) + (y_j)_x(t)\phi_{2j}(x)].$$

An advantage of this choice of discrete space and its basis is that it yields the simple relations:

$$y_h(1, t) = y_{N-1}(t), (y_h)_x(1, t) = y_N(t).$$

Then, the finite element approximation of (1.1)-(1.3) consists in finding $\hat{y}_h = (y_h(1), (y_h)_x(1), y_h) \in C^2([0, \infty); \mathbb{Y})$ or $y_h \in C^2([0, \infty); V^h)$ for all $t > 0$ and satisfies

$$\int_0^1 m(y_h)_{tt} \phi_j \, dx + \int_0^1 EI(y_h)_{xx}(\phi_j)_{xx} \, dx + \int_0^1 \gamma(y_h)_t \phi_j \, dx = 0 \tag{2.3}$$

for all $j = 1, \dots, N$ and $t > 0$. So we look for the solution y_h in the form: $y_h(x, t) = \sum_{i=1}^N y_i(t)\phi_i(x)$ where $y_i(t)$ are the unknown coefficients and $N = 2n$ is the dimension of V^h . In other words, we have:

$$\sum_{i=1}^N \int_0^1 m(y_i)_{tt} \phi_i \phi_j \, dx + \sum_{i=1}^N \int_0^1 EI(y_i)_{xx}(\phi_i)_{xx}(\phi_j)_{xx} \, dx + \sum_{i=1}^N \int_0^1 \gamma(y_i)_t \phi_i \phi_j \, dx = 0,$$

for all $i, j = 1, \dots, N$ and $t > 0$, with initial conditions

$$y_h(0, \cdot) = y_{h,0} \in V^h, \quad (y_h)_t(0, \cdot) = v_{h,0} \in V^h.$$

By noting $Y(t)$ the vector representation of the function y_h defined as follows:

$$Y = [y_1, y_2, \dots, y_N]^T,$$

(2.3) can be written by

$$MY_{tt} + BY_t + KY = 0. \tag{2.4}$$

The matrices M , B , and K are defined by

$$K_{ij} = \int_0^1 EI(\phi_i)_{xx}(\phi_j)_{xx} \, dx, \quad B_{ij} = \int_0^1 \gamma \phi_i \phi_j \, dx, \quad M_{ij} = \int_0^1 m \phi_i \phi_j \, dx, \quad \forall i, j = 1, \dots, N.$$

M is the mass matrix, B is the viscous damping matrix, and K the rigidity matrix.

- K is symmetric, defined, and positive because $EI > 0$ therefore K is invertible.
- The matrix M is also symmetric, defined, and positive therefore M is invertible. Using the theory of linear differential equations, the problem (2.4) has a unique solution. This implies the existence and the uniqueness of the solution of (2.3).

2.3.2. A-priori error estimates

In this subsection, the a-priori error estimates for the Galerkin solution of (2.3) shall be derived. V^h is the space of Hermite cubic polynomials as described above. The classical method of obtaining the error estimates presented in [5] is used. Since the Hermite cubic polynomials are used as an approximation space, the order precision in space ($H^2(0, 1)$) is obtained. The Hermite interpolation of the weak solution y of V^h on \mathbb{V} denoted by \tilde{y} is defined as follows:

$$\forall x \in (0, 1), \forall t > 0, \tilde{y}(x, t) = \sum_{i=1}^n y(x_i, t)\phi_{2i-1}(x) + \sum_{i=1}^n y_x(x_i, t)\phi_{2i}(x).$$

In addition, we make the following assumptions:

$$y \in C([0, T]; G), \quad y_t \in L^2(0, T; G), \quad y_{tt} \in L^2(0, T; \mathbb{V}), \tag{2.5}$$

with

$$G = \{y \in H^4(0, 1), \quad y(0) = y_x(0) = 0\}.$$

Then for almost every t , we have following [5]:

$$\|y - \tilde{y}\|_{H^2(0,1)} \leq Ch^2\|y\|_{H^4(0,1)}, \quad \|y_t - \tilde{y}_t\|_{H^2(0,1)} \leq Ch^2\|y_t\|_{H^4(0,1)}, \tag{2.6}$$

and according to Theorem 5.4.8 of [4], we have:

$$\|y_{tt} - \tilde{y}_{tt}\|_{L^2(0,1)} \leq Ch^2\|y_{tt}\|_{H^2(0,1)}. \tag{2.7}$$

Then, the convergence theorem of the semi-discretized scheme is as follows.

Theorem 2.4. *Let V^h be the space of cubic Hermite polynomials. Assume the expressions (2.5) hold. The following error estimate holds for $y_h \in C^2([0, T]; V^h)$, solution of (2.3),*

$$\forall t \in [0, T], \left[\mathbb{E}(t, y_h - y) \right]^{1/2} \leq K \left(\mathbb{E}(0, y_h(0) - y(0))^{1/2} + h^2 (\|y\|_{C([0,T];H^4(0,1))} + \|y_t\|_{L^2(0,T;H^4(0,1))} + \|y_{tt}\|_{L^2(0,T;H^4(0,1))}) \right). \tag{2.8}$$

In addition, if y_{h0} and z_{h0} are Hermite interpolations of y_0 and z_0 , then there exists a positive constant K such that:

$$\left[\mathbb{E}(t, y_h - y) \right]^{1/2} \leq Kh^2 \left(\|y\|_{C([0,T];H^4(0,1))} + \|y_t\|_{L^2(0,T;H^4(0,1))} + \|y_{tt}\|_{L^2(0,T;H^4(0,1))} \right). \tag{2.9}$$

Remark 2.5. The order of convergence for the discretized scheme in space is 2.

Proof of Theorem 2.4. The error of the semi-discrete solution y_h is defined as $e_h = y_h - \tilde{y}$. Utilizing equation (2.3), we get:

$$\begin{aligned} & \int_0^1 m(e_h)_{tt}\phi \, dx + \int_0^1 EI(e_h)_{xx}\phi_{xx} \, dx + \int_0^1 \gamma(e_h)_t(x)\phi \, dx \\ & = \int_0^1 m(y - \tilde{y})_{tt}\phi \, dx + \int_0^1 EI(y - \tilde{y})_{xx}\phi_{xx} \, dx + \int_0^1 \gamma(y - \tilde{y})_t\phi \, dx, \end{aligned} \tag{2.10}$$

for all $\phi \in V^h$ and for all $t > 0$. Using $\phi = (e_h)_t \in V^h$, (2.10) gives:

$$\begin{aligned} & \int_0^1 m(e_h)_{tt}(e_h)_t \, dx + \int_0^1 EI(e_h)_{xx}(e_h)_{xxt} \, dx + \int_0^1 \gamma(e_h)_t(x)(e_h)_t \, dx \\ & = \int_0^1 m(y - \tilde{y})_{tt}(e_h)_t \, dx + \int_0^1 EI(y - \tilde{y})_{xx}(e_h)_{xxt} \, dx + \int_0^1 \gamma(y - \tilde{y})_t(e_h)_t \, dx, \forall t \in [0, T]. \end{aligned}$$

As a result, for almost every $t \in [0, T]$,

$$\begin{aligned} \frac{1}{2} \frac{d}{dt} \left[\int_0^1 m(e_h)_t^2 dx + \int_0^1 EI(e_h)_{xx}^2 dx \right] &= \int_0^1 m(y - \tilde{y})_{tt}(e_h)_t dx + \int_0^1 EI(y - \tilde{y})_{xx}(e_h)_{txx} dx \\ &+ \int_0^1 \gamma(y - \tilde{y})_t(x)(e_h)_t dx, - \int_0^1 \gamma(e_h)_t(x)(e_h)_t dx. \end{aligned}$$

This implies that:

$$\frac{1}{2} \frac{d}{dt} \mathbb{E}(t, e_h) \leq \int_0^1 m(y - \tilde{y})_{tt}(e_h)_t dx + \int_0^1 EI(y - \tilde{y})_{xx}(e_h)_{txx} dx + \int_0^1 \gamma(y - \tilde{y})_t(e_h)_t dx, \tag{2.11}$$

for almost every $t \in [0, T]$. Integrating the expression (2.11) in time, we obtain

$$\begin{aligned} \mathbb{E}(t, e_h) &\leq \mathbb{E}(0, e_h(0)) + 2 \int_0^t \int_0^1 m(y - \tilde{y})_{tt}(e_h)_t dx dv \\ &+ 2 \int_0^t \int_0^1 EI(y - \tilde{y})_{xx}(e_h)_{txx} dx dv + \int_0^t \int_0^1 \gamma(y - \tilde{y})_t(e_h)_t dx dv. \end{aligned} \tag{2.12}$$

In expression (2.12), we integrate by parts $\int_0^t EI(y - \tilde{y})_{xx}(e_h)_{txx} dv$. It follows for almost every $t \in [0, T]$:

$$\begin{aligned} \mathbb{E}(t, e_h) &\leq \mathbb{E}(0, e_h(0)) + 2 \int_0^t \int_0^1 \gamma(y_t(x, v) - \tilde{y}_t(x, v))(e_h)_t(x, v) dx dv \\ &+ 2 \int_0^t \int_0^1 m(y_{tt}(x, v) - \tilde{y}_{tt}(x, v))(e_h)_t(x, v) dx dv \\ &- 2 \int_0^t \int_0^1 EI(y_{txx}(x, v) - \tilde{y}_{txx}(x, v))(e_h)_{xx}(x, v) dx dv \\ &+ 2 \int_0^1 EI(y_{xx}(x, t) - \tilde{y}_{xx}(x, t))(e_h)_{xx}(x, t) dx \\ &+ 2 \int_0^1 EI(y_{xx}(x, 0) - \tilde{y}_{xx}(x, 0))(e_h)_{xx}(x, 0) dx. \end{aligned} \tag{2.13}$$

Applying Cauchy-Schwarz to (2.13) yields:

$$\begin{aligned} \mathbb{E}(t, e_h) &\leq \mathbb{E}(0, e_h(0)) + \tilde{m} \left[\|y_{tt} - \tilde{y}_{tt}\|_{L^2(0,T;L^2(0,1))}^2 + \int_0^t \|(e_h)_t(\cdot, v)\|_{L^2(0,1)}^2 dv \right] \\ &+ \tilde{\gamma} \left[\|y_t - \tilde{y}_t\|_{L^2(0,T;L^2(0,1))}^2 + \int_0^t \|(e_h)_t(\cdot, v)\|_{L^2(0,1)}^2 dv \right] \\ &+ \tilde{EI} \left[\|y_t - \tilde{y}_t\|_{L^2(0,T;H^2(0,1))}^2 + \int_0^t \|(e_h)_{xx}(\cdot, v)\|_{L^2(0,1)}^2 dv \right] \\ &+ 8\tilde{EI} \left[\|y_{xx}(\cdot, t) - \tilde{y}_{xx}(\cdot, t)\|_{L^2(0,1)}^2 + \frac{1}{64} \|(e_h)_{xx}(\cdot, t)\|_{L^2(0,1)}^2 \right] \\ &+ 8\tilde{EI} \left[\|y_{xx}(\cdot, 0) - \tilde{y}_{xx}(\cdot, 0)\|_{L^2(0,1)}^2 + \frac{1}{64} \|(e_h)_{xx}(\cdot, 0)\|_{L^2(0,1)}^2 \right], \end{aligned}$$

where $\tilde{\gamma} := \max_{x \in [0,1]} \gamma(x)$, $\tilde{m} := \max_{x \in [0,1]} m(x)$, and $\tilde{EI} := \max_{x \in [0,1]} EI(x)$. Using the estimations (2.6)-(2.7), it follows:

$$\mathbb{E}(t, e_h) \leq M_1 \mathbb{E}(0, e_h(0)) + M_2 \int_0^t \mathbb{E}(v, e_h) dv + Mh^4 \left(\|y\|_{C([0,T];H^4(0,1))}^2 \right)$$

$$+ \|y_t\|_{L^2(0,T;H^4(0,1))}^2 + \|y_{tt}\|_{L^2(0,T;H^2(0,1))}^2),$$

where M_1, M_2 , and M denote constants. Gronwall’s inequality applied to the last inequality gives

$$\mathbb{E}(t, e_h) \leq K \left(\mathbb{E}(0, e_h(0)) + h^4 \left(\|y\|_{C([0,T];H^4(0,1))}^2 + \|y_t\|_{L^2(0,T;H^4(0,1))}^2 + \|y_{tt}\|_{L^2(0,T;H^2(0,1))}^2 \right) \right).$$

Using the triangular inequality, we obtain (2.8). Finally, from (2.8) with $e_h(0) = 0$, (2.9) is verified. □

2.4. Fully-discrete scheme: time discretization

We now turn to the study the fully discretization in time using Crank-Nicolson scheme, based on the semi-discretization (2.3) we just did. Lastly, the a-priori error estimated is obtained.

2.4.1. Crank-Nicolson scheme

For a fixed real $T > 0$, we subdivide the interval $[0, T]$ into S intervals of the same length $\Delta t := T/S$. We then set at any point $t_n = n\Delta t$ the nodes of the discretization for all $0 \leq n \leq S$. For the time discretization of (2.3), the Crank-Nicolson scheme is used

$$\frac{y^{n+1} - y^n}{\Delta t} = \frac{z^{n+1} + z^n}{2}. \tag{2.14}$$

The equation (2.3) can be written as

$$\int_0^1 m \frac{z^{n+1} - z^n}{\Delta t} \phi_h dx + \int_0^1 \gamma \frac{z^{n+1} + z^n}{2} \phi_h dx + \int_0^1 EI \frac{y_{xx}^{n+1} + y_{xx}^n}{2} (\phi_h)_{xx} dx = 0, \tag{2.15}$$

for all $\phi_h \in V^h$. The Crank-Nicolson scheme for the equation (2.4) becomes the vector equation

$$\frac{MZ^{n+1} - MZ^n}{\Delta t} + \frac{BZ^{n+1} + BZ^n}{2} + \frac{KY^{n+1} + KY^n}{2} = 0, \tag{2.16}$$

where $Y^n = Y(t_n, x)$ and $Z^n = Z(t_n, x)$ are the vector representations of y^n and z^n in the considered basis V^h , respectively. Note that $Z = Y_t = [Z_1 \ Z_2 \ \dots \ Z_N]^T$ is the vector representation in the basis $\{\phi_j\}_{j=1}^N$. Equation (2.16) is written in the following form:

$$\left(\frac{M}{\Delta t} + \frac{B}{2} \right) Z^{n+1} + \frac{K}{2} Y^{n+1} = -\frac{K}{2} Y^n + \left(\frac{M}{\Delta t} - \frac{B}{2} \right) Z^n. \tag{2.17}$$

The equations (2.14) and (2.17) are written in a compact vector form:

$$SW^{n+1} = FW^n,$$

where S and F are defined by:

$$S = \begin{pmatrix} \frac{I}{\Delta t} & -\frac{I}{2} \\ \frac{K}{2} & \frac{M}{\Delta t} + \frac{B}{2} \end{pmatrix}, \quad F = \begin{pmatrix} \frac{I}{\Delta t} & \frac{I}{2} \\ -\frac{K}{2} & \frac{M}{\Delta t} - \frac{B}{2} \end{pmatrix},$$

and the vector W^n is defined by $W^n = [Y^n \ Z^n]$.

Theorem 2.6. *The fully discrete scheme (2.15) has a unique solution.*

Notation: For any sequence $\{x_n\} \subset \mathbb{R}^n$, set

$$\delta_t x_n = \frac{x_{n+1} - x_n}{\Delta t}, \quad x_{n+1/2} = \frac{x_{n+1} + x_n}{2}.$$

Define a bilinear form $c(\cdot, \cdot)$ over $L^2(0, 1) \times L^2(0, 1)$ by setting

$$c(u, v) = \int_0^1 m(x)u(x)v(x) dx \quad \forall u, v \in L^2(0, 1).$$

We reformulate the fully discrete problem in order to justify the existence. The problem is referred to as Problem E^h .

Problem 2.7 (Problem E^h). Find a sequence $\{y_n\} \subset V^h$ such that for $n \in \{0, 1, \dots, S-1\}$,

$$\delta_t y_n = z_{n+1/2}, \tag{2.18}$$

$$c(\delta_t z_n, \psi) + a_2(z_{n+1/2}, \psi) + a_1(y_{n+1/2}, \psi) = 0, \tag{2.19}$$

for all $\psi \in V^h$, with $y_n(0) = y_0^n = d^n$ and $(y_n)_t(0) = y_1^n = e^n$.

Proposition 2.8. *Problem E^h has a unique solution for any pair of vectors d^n and e^n in V^h .*

Proof. For any $\psi \in V^h$,

$$\begin{aligned} \frac{\Delta t}{2} a_1(y_{n+1} + y_n, \psi) &= \frac{\Delta t^2}{2} a_1(\Delta t^{-1}[y_{n+1} - y_n], \psi) + \frac{\Delta t}{2} a_1(y_n, \psi) + \frac{\Delta t}{2} a_1(y_n, \psi) \\ &= \frac{\Delta t^2}{4} a_1(z_{n+1}, \psi) + \frac{\Delta t^2}{4} a_1(z_n, \psi) + \Delta t a_1(y_n, \psi). \end{aligned}$$

Substitution into (2.19), we obtain

$$\begin{aligned} c(z_{n+1}, \psi) + \frac{\Delta t}{2} a_2(z_{n+1}) + \frac{\Delta t^2}{4} a_1(z_{n+1}, \psi) \\ = c(z_n, \psi) - \frac{\Delta t}{2} a_2(z_n, \psi) - \frac{\Delta t^2}{4} a_1(z_n, \psi) - \Delta t a_1(y_n, \psi) \end{aligned} \tag{2.20}$$

for any $\psi \in V^h$. The bilinear forms a_1 and c are positive definite and as a consequence $c + \frac{\Delta t}{2} a_2 + \frac{\Delta t^2}{4} a_1$ is positive definite. Therefore, z_{n+1} is uniquely determined by (2.20) and $y_{n+1} = y_n + \Delta t z_{n+1/2}$ of (2.18). \square

2.4.2. A-priori error estimates

In this subsection, a-priori error estimates for the fully discretized scheme are obtained. Suppose that $y \in H^4(0, T; \mathbb{V})$. $\bar{y} \in V^h$ denotes the projection of the weak solution y on V^h such that

$$a_1(\bar{y}(t), \phi_h) = a_1(y(t), \phi_h),$$

$\forall \phi_h \in V^h, \forall t \in [0, T]$. Since the projection \bar{y} is bounded in \mathbb{V} , then we have $\bar{y} \in H^4(0, T; \mathbb{V})$. In addition, we denote by $y^e = y - \bar{y}$ the projection error. Suppose also that

$$y \in H^2(0, T; H^4_{\mathbb{E}}(0, 1)), \quad y_t \in L^2(0, T; H^4_{\mathbb{E}}(0, 1)), \quad y_{tt} \in H^2(0, T; \mathbb{V}).$$

Following [14], we have:

$$\begin{aligned} \|y - \bar{y}\|_{H^2(0,1)} &\leq Ch^2 \|y\|_{H^4(0,1)}, \\ \|y_t - \bar{y}_t\|_{H^2(0,1)} &\leq Ch^2 \|y_t\|_{H^4(0,1)}, \\ \|y_{tt} - \bar{y}_{tt}\|_{H^2(0,1)} &\leq Ch^2 \|y_{tt}\|_{H^4(0,1)}. \end{aligned} \tag{2.21}$$

Let $w(t_n) = [y(t_n) \ y_t(t_n)]^T$ denote the weak solution of (2.2) at time $t = t_n$ and $w^n = [y^n \ z^n]^T$, the n^{th} iteration of the fully discrete scheme (2.16)-(2.17), approximating $w(t_n)$. Thus, the approximation error is defined by

$$\varphi^n = y^n - \bar{y}(t_n), \quad \xi^n = z^n - \bar{y}_t(t_n), \quad \text{and} \quad w_e^n = [\varphi^n \ \xi^n]^T,$$

for every $n = 0, 1, \dots, S$.

The following theorem gives the second order error estimate of the fully discrete scheme.

Theorem 2.9. Assume $y \in H^2([0, T]; H^4_x(0, 1)) \cap H^4([0, T]; \mathbf{V})$. For $n \in \{1, \dots, S\}$, we have the following result:

$$\|w^n - w(t_n)\| \leq \widehat{C} \left[\|w_e^0\| + h^2 \|y\|_{H^2([0, T]; H^4(0, 1))} + (\Delta t)^2 \left(\|y_{tt}\|_{L^2([0, T]; H^4(0, 1))} + \|y_{tt}\|_{H^2([0, T]; H^2(0, 1))} \right) \right],$$

where \widehat{C} is a positive constant.

Proof. Let's arbitrarily take $n = 0, 1, \dots, S$ with S a strictly positive integer. Using Taylor's Theorem with integral remainder and by direct calculation, we obtain the two following expressions, for all $x \in [0, 1]$. On the one hand,

$$\frac{\bar{y}(x, t_{n+1}) - \bar{y}(x, t_n)}{\Delta t} = \bar{y}_t(x, t_{n+1/2}) + \frac{1}{\Delta t} \int_{t_{n+1/2}}^{t_{n+1}} \frac{(t_{n+1} - t)^2}{2} \bar{y}_{ttt}(x, t) dt + \frac{1}{\Delta t} \int_{t_n}^{t_{n+1/2}} \frac{(t_n - t)^2}{2} \bar{y}_{ttt}(x, t) dt.$$

On the other hand, we have

$$\frac{\bar{y}_t(x, t_{n+1}) + \bar{y}_t(x, t_n)}{2} = \bar{y}_t(x, t_{n+1/2}) + \frac{1}{2} \int_{t_{n+1/2}}^{t_{n+1}} (t_{n+1} - t) \bar{y}_{ttt}(x, t) dt - \frac{1}{2} \int_{t_n}^{t_{n+1/2}} (t_n - t) \bar{y}_{ttt}(x, t) dt.$$

From these two previous expressions, we obtain:

$$\frac{\bar{y}(x, t_{n+1}) - \bar{y}(x, t_n)}{\Delta t} = \frac{\bar{y}_t(x, t_{n+1}) + \bar{y}_t(x, t_n)}{2} + \Delta t U_1^n(x), \tag{2.22}$$

where

$$U_1^n(x) = \frac{1}{2} \int_{t_{n+1/2}}^{t_{n+1}} (t_{n+1} - t)^2 \frac{\bar{y}_{ttt}(x, t)}{\Delta t^2} dt + \frac{1}{2} \int_{t_n}^{t_{n+1/2}} (t_n - t)^2 \frac{\bar{y}_{ttt}(x, t)}{\Delta t^2} dt - \frac{1}{2} \int_{t_{n+1/2}}^{t_{n+1}} (t_{n+1} - t) \frac{\bar{y}_{ttt}(x, t)}{\Delta t} dt + \frac{1}{2} \int_{t_n}^{t_{n+1/2}} (t_n - t) \frac{\bar{y}_{ttt}(x, t)}{\Delta t} dt.$$

Using (2.22) yields

$$\frac{\varphi^{n+1} - \varphi^n}{\Delta t} = \frac{\xi^{n+1} + \xi^n}{2} - \Delta t U_1^n(x). \tag{2.23}$$

Furthermore, in order to rewrite the weak formulation (2.11), we obtain by the Taylor's theorem with integral remainder, the following expressions:

$$\begin{aligned} \frac{y_t(x, t_{n+1}) - y_t(x, t_n)}{\Delta t} &= y_{tt}(x, t_{n+1/2}) + \frac{1}{2} \int_{t_{n+1/2}}^{t_{n+1}} \frac{(t_{n+1} - t)^2}{\Delta t} y_{tttt}(x, t) dt \\ &\quad + \frac{1}{2} \int_{t_n}^{t_{n+1/2}} \frac{(t_n - t)^2}{\Delta t} y_{tttt}(x, t) dt, \end{aligned}$$

and

$$\frac{y_{xx}(x, t_{n+1}) + y_{xx}(x, t_n)}{2} = y_{xx}(x, t_{n+1/2}) + \frac{1}{2} \int_{t_{n+1/2}}^{t_{n+1}} (t_{n+1} - t) y_{ttxx}(x, t) dt$$

$$-\frac{1}{2} \int_{t_n}^{t_{n+1/2}} (t_n - t) y_{ttxx}(x, t) dt.$$

Replacing t by $t_{n+1/2}$ and applying the previous expressions to the weak formulation (2.11), we obtain:

$$\begin{aligned} & \int_0^1 m \left(\frac{y_t(x, t_{n+1}) - y_t(x, t_n)}{\Delta t} \right) \phi dx + \int_0^1 EI \left(\frac{y_{xx}(x, t_{n+1}) + y_{xx}(x, t_n)}{2} \right) \phi_{xx} dx \\ & + \int_0^1 \gamma \left(\frac{y_t(x, t_{n+1}) + y_t(x, t_n)}{2} \right) \phi dx = \Delta t U_2^n(\phi), \end{aligned} \tag{2.24}$$

where

$$\begin{aligned} U_2^n(\phi) = & \int_0^1 m \left(\frac{1}{2} \int_{t_{n+1/2}}^{t_{n+1}} \frac{y_{tttt}(x, t)}{\Delta t^2} (t_{n+1} - t)^2 dt + \frac{1}{2} \int_{t_n}^{t_{n+1/2}} \frac{y_{tttt}(x, t)}{\Delta t^2} (t_n - t)^2 dt \right) \phi dx \\ & + \int_0^1 EI \left(\frac{1}{2} \int_{t_{n+1/2}}^{t_{n+1}} \frac{y_{ttxx}(x, t)}{\Delta t} (t_{n+1} - t) dt - \frac{1}{2} \int_{t_n}^{t_{n+1/2}} \frac{y_{ttxx}(x, t)}{\Delta t} (t_n - t) dt \right) \phi_{xx} dx \\ & + \int_0^1 \gamma \left(\frac{1}{2} \int_{t_{n+1/2}}^{t_{n+1}} \frac{y_{ttt}(x, t)}{\Delta t} (t_{n+1} - t) dt - \frac{1}{2} \int_{t_n}^{t_{n+1/2}} \frac{y_{ttt}(x, t)}{\Delta t} (t_n - t) dt \right) \phi dx \end{aligned}$$

and is defined as follows $U_2^n : V \rightarrow \mathbb{R}$. Now, from (2.24) and (2.15), we have for all $\phi_h \in V^h$,

$$\begin{aligned} & \int_0^1 m \frac{\xi^{n+1} - \xi^n}{\Delta t} \phi_h dx + \int_0^1 EI \frac{\varphi_{xx}^{n+1} + \varphi_{xx}^n}{2} (\phi_h)_{xx} dx + \int_0^1 \gamma \frac{\xi^{n+1} + \xi^n}{2} \phi_h dx \\ & = -\Delta t U_2^n(\phi_h) + U_3^n(\phi_h), \end{aligned} \tag{2.25}$$

where

$$U_3^n(\phi_h) = \int_0^1 m \frac{y_t^e(x, t_{n+1}) - y_t^e(x, t_n)}{\Delta t} \phi_h dx + \int_0^1 \gamma \frac{y_t^e(x, t_{n+1}) + y_t^e(x, t_n)}{2} \phi_h dx. \tag{2.26}$$

Using (2.23) and taking $\phi_h = \Delta t \frac{\xi^{n+1} + \xi^n}{2} \in V^h$ in (2.25), we obtain:

$$\begin{aligned} \|w_e^{n+1}\|^2 - \|w_e^n\|^2 = & -\Delta t^2 \int_0^1 EI \frac{\varphi_{xx}^{n+1} + \varphi_{xx}^n}{2} (U_1^n)_{xx} dx \\ & - \int_0^1 \gamma \frac{\xi^{n+1} + \xi^n}{2} \times \frac{\Delta t}{2} dx - \frac{\Delta t^2}{2} U_2^n(\xi^{n+1} + \xi^n) + \frac{\Delta t}{2} U_3^n(\xi^{n+1} + \xi^n). \end{aligned}$$

The following estimate is used

$$\|U_1^n\|_{H^2}^2 \leq \Delta t \int_{t_n}^{t_{n+1}} \|\bar{y}_{ttt}(t)\|_{H^2}^2 dt \leq \widehat{C} \Delta t \int_{t_n}^{t_{n+1}} \|y_{ttt}(t)\|_{H^2}^2 dt.$$

Rewriting the second term of $U_2^n(\xi^n)$ (using the fact that $\xi^n(0) = \xi_x^n(0) = 0$) and integrating twice by parts over $[0, 1]$, we get:

$$\begin{aligned} & \int_0^1 \left(\frac{1}{2} \int_{t_{n+1/2}}^{t_{n+1}} \frac{y_{ttxx}(x, t)}{\Delta t} (t_{n+1} - t) dt - \frac{1}{2} \int_{t_n}^{t_{n+1/2}} \frac{y_{ttxx}(x, t)}{\Delta t} (t_n - t) dt \right) \xi_{xx}^n dx \\ & = \int_{t_{n+1/2}}^{t_{n+1}} \frac{1}{2\Delta t} (t_{n+1} - t) \left(y_{ttxx}(1, t) \xi_x^n(1) - y_{ttxxx}(1, t) \xi^n(1) + \int_0^1 y_{ttxxx}(1, t) \xi^n dx \right) dt \end{aligned}$$

$$-\int_{t_n}^{t_{n+1/2}} \frac{1}{2\Delta t} (t_n - t) \left(y_{ttxx}(1, t) \xi_x^n(1) - y_{ttxxx}(1, t) \xi^n(1) + \int_0^1 y_{ttxxx}(1, t) \xi^n dx \right) dt.$$

Then

$$|U_2^n(\xi^n)| \leq \widehat{C} \left(\Delta t \int_{t_n}^{t_{n+1}} \|y_{tttt}(t)\|_{H^2}^2 + \|y_{ttt}(t)\|_{H^2}^2 + \|y_{tt}(t)\|_{H^4}^2 dt + \|\xi^n\|_{L^2}^2 + |\xi_x^n(1)|^2 + |\xi^n(1)|^2 \right).$$

Moreover, from (2.26) we have:

$$|U_3^n(\xi^{n+1} + \xi^n)| \leq \widehat{C} \left(\frac{1}{\Delta t} \int_{t_n}^{t_{n+1}} \|y_{tt}^e(t)\|_{L^2}^2 + \|y_t^e(t)\|_{C([t_n, t_{n+1}], H^2)}^2 + \|\xi^{n+1} + \xi^n\|_{L^2}^2 + |\xi_x^{n+1}(1) + \xi_x^n(1)|^2 \right).$$

We deduce that

$$\begin{aligned} \|w_e^{n+1}\|^2 - \|w_e^n\|^2 &\leq \widehat{C} \left(\Delta t (\|w_e^{n+1}\|^2 + \|w_e^n\|^2 + \|y_t^e\|_{C([t_n, t_{n+1}], H^2)}^2) \right. \\ &\quad \left. + \int_{t_n}^{t_{n+1}} \|y_{tt}^e(t)\|_{L^2}^2 dt + \Delta t^4 \int_{t_n}^{t_{n+1}} \|y_{tt}(t)\|_{H^4}^2 + \|y_{ttt}(t)\|_{H^2}^2 + \|y_{tttt}(t)\|_{H^2}^2 dt \right). \end{aligned}$$

Let $m = 1, \dots, S$. Summing on $n = 0, \dots, m$ and supposing that $\Delta t \leq \frac{1}{2\widehat{C}}$, finally, using the discrete-in-time Gronwall inequality and the estimates (2.21), we obtain:

$$\begin{aligned} \|w_e^{m+1}\|^2 &\leq \widehat{C} \left[\|w_e^0\|^2 + h^4 \left(\|y_t\|_{C([0, T], H^4)}^2 + \|y_{tt}\|_{L^2([0, T], H^4)}^2 \right) \right. \\ &\quad \left. + (\Delta t)^4 \left(\|y_{tt}(t)\|_{L^2([0, T], H^4)}^2 + \|y_{ttt}(t)\|_{L^2([0, T], H^2)}^2 + \|y_{tttt}(t)\|_{L^2([0, T], H^2)}^2 \right) \right]. \end{aligned}$$

Using the triangle inequality the result now follows. □

3. Numerical results

3.1. Uniform case with constant damping γ

In this section, we present some numerical simulation results by the approximation method presented in this paper. The numerical results provided in this section verify the prediction Theorem 2.2. Let $m = EI = 1$. Moreover, we take the time step $\Delta t = 0.01$ and the spatial discretization $h = 0.01$. The initial conditions are taken as follows:

$$y_0(x) = 0.4x^3 - 0.6x^2 \quad \text{and} \quad z_0 \equiv 0.$$

3.1.1. Representation of the deflection and energy

The simulations are performed for three different cases: a) $\gamma = 0.1$; b) $\gamma = 1$; and c) $\gamma = 10$. Figures 1, 2, and 3 represent the deflection of beam $y(x, t)$ for cases a) b), and c), respectively. Figure 4 represents the decay of energy function on the time interval $[0, 50]$ for cases a), b), and c), respectively. We can deduce that the quick decay of energy is related to large values of γ .

3.1.2. Representation of tip position $y(1, t)$ and tip angle $y_x(1, t)$

In the Figures 5 and 6, tip position $y(1, t)$ and tip angle of the beam $y_x(1, t)$ are compared on time interval $[0, 50]$. In Figures 5 and 6, we notice that, when the value of γ gets great the vibrations of the beams tip are suppressed, also we observe a quickly convergence to the steady-state.

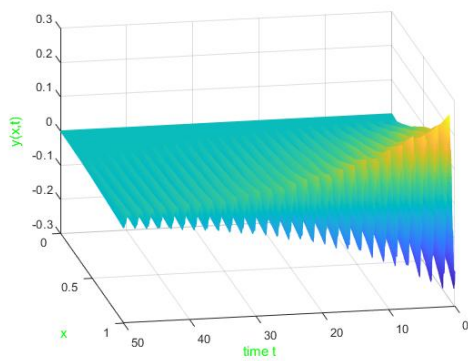


Figure 1: Deflection $y(x, t)$.

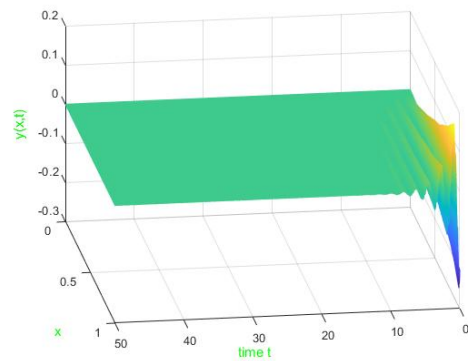


Figure 2: Deflection $y(x, t)$.

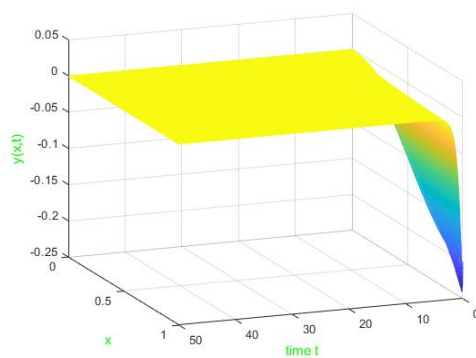


Figure 3: Deflection $y(x, t)$.

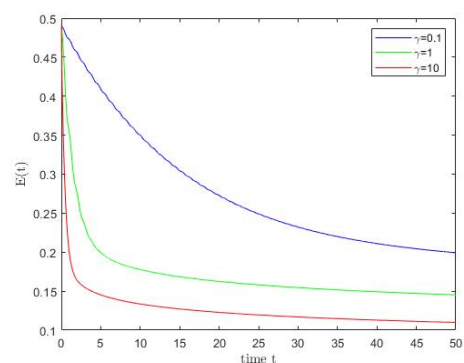


Figure 4: Influence of the damping γ on the energy.

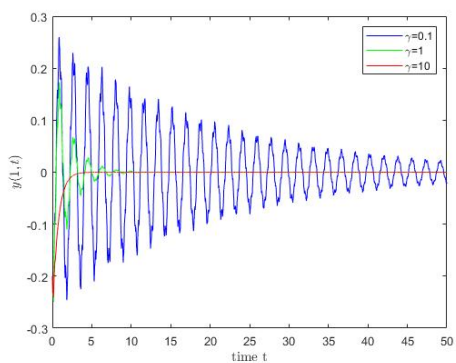


Figure 5: Tip position comparison.

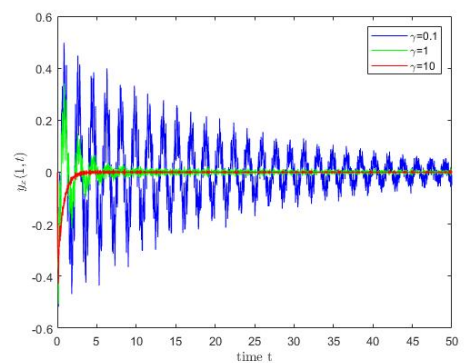


Figure 6: Tip angle comparison.

3.1.3. Study of the spectrum

As mentioned above, we use the finite element method to numerically solve the spectrum. We have to solve the following equation (2.4) in \mathbb{R}^N with unknown $Y(t)$. Let's put $Z = Y_t$ and $U = [Y \ Y_t]^T$, the equation (2.4) is written as $U_t(t) = LU(t)$, where

$$L = \begin{pmatrix} 0 & I \\ -M^{-1}K & -M^{-1}B \end{pmatrix}$$

is the spectrum matrix. Now, by implementing the spectrum matrix L , we represent the spectrum associated with the system (1.1)-(1.3) for $N = 75$ and for different values of γ . On the Figure 7, we have represented a distribution of $4N$ eigenvalues for different values of γ .

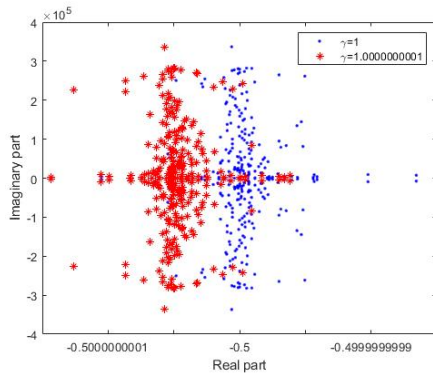


Figure 7: Influence of the variation of the damping γ on the spectrum.

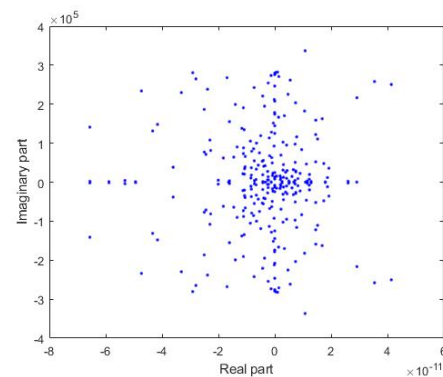


Figure 8: Representation of spectrum, when $\gamma = 0$.

We notice a spectrum family whose real part is negative. This makes the system exponentially stable as long as $\gamma > 0$. We certainly see a scattered spectrum but contained in the left complex plane. This is due to the fact that the system is not controlled. Also, we observe a shift of the spectrum to the left for large values of damping. To observe on the same graph this representation, the values must be very close. We observe the behaviour of the system when $\gamma = 0$ (Figure 8). We observe a spectrum scattered on both sides of the imaginary axis. This leads to believe that the system is not uniformly stable when $\gamma = 0$. We also illustrate the asymptote for uniform case:

$$\lim_{n \rightarrow \infty} \operatorname{Re} \lambda_n = \frac{-1}{2h} \int_0^1 \gamma(x) dx.$$

In Figures 9 and 10, we plot the spectrum with respect to the above asymptote. We plot the spectrum for $\gamma = 1$, we observe the asymptote at the spectral abscissa -0.5 . We have the representation of the spectrum for $\gamma = 5$ with respect to the asymptote at the spectral abscissa -2.5 .

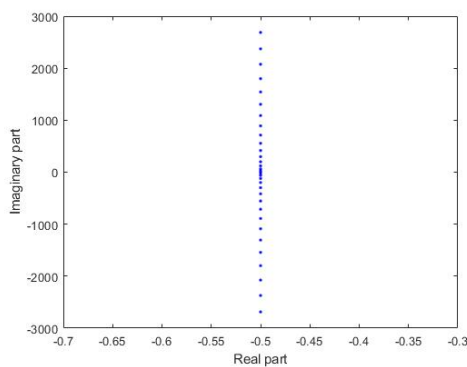


Figure 9: Asymptote of the spectrum for $\gamma = 1$.

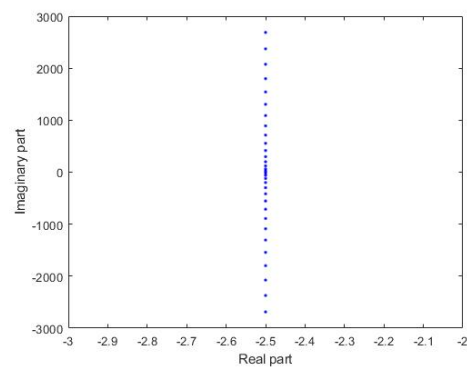


Figure 10: Asymptote of the spectrum for $\gamma = 5$.

3.2. Uniform case with variable damping γ

We present some numerical simulation results for variable γ .

3.2.1. Representation of the deflection and energy

The simulations are performed for three different cases: a) $\gamma(x) = (1 + x)^2$; b) $\gamma(x) = (1 + x)^3$; and c) $\gamma(x) = (1 + x)^4$. Figures 11, 12, and 13 represent the deflection of beam $y(x, t)$ for cases a), b), and c), respectively. Figure 14 represents the decay of energy function $\mathbb{E}(t)$ on the time interval $[0, 50]$ for cases a), b), and c), respectively. We can deduce that the quick decay of energy is related to large values of γ .

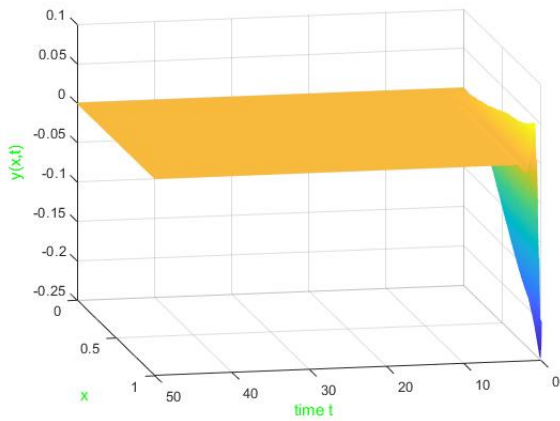


Figure 11: Deflection $y(x, t)$.

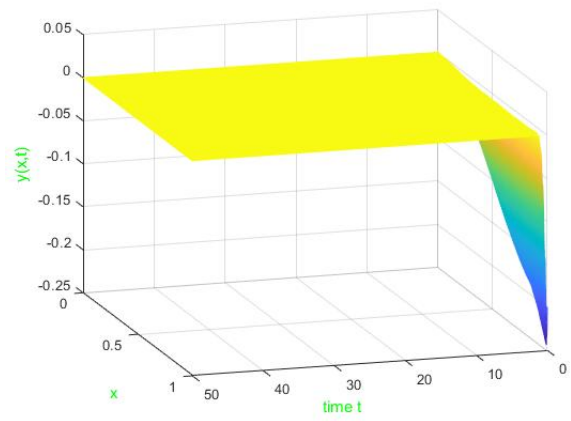


Figure 12: Deflection $y(x, t)$.

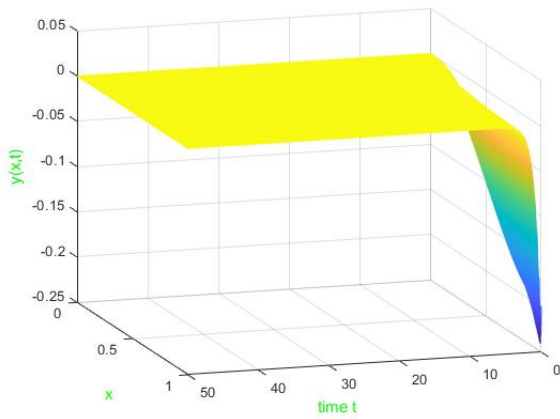


Figure 13: Deflection $y(x, t)$.

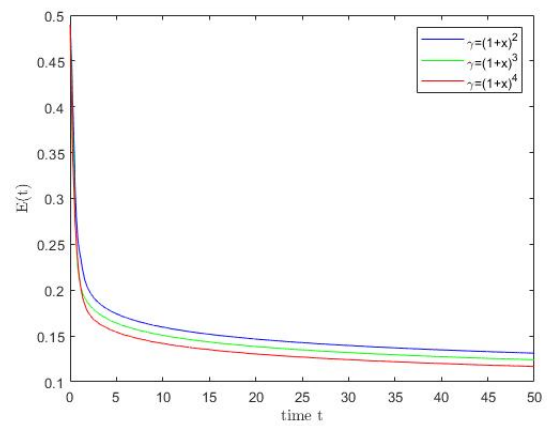


Figure 14: Influence of the damping γ on the energy.

3.2.2. Representation of Tip position $y(1, t)$ and Tip angle $y_x(1, t)$

In the Figures 15 and 16, tip position $y(1, t)$ and tip angle of the beam $y_x(1, t)$ are compared on time interval $[0, 50]$.

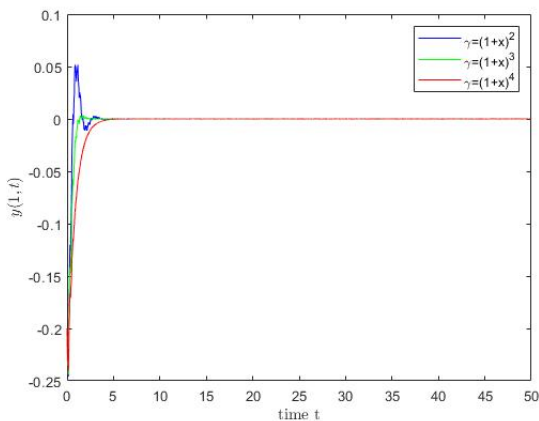


Figure 15: Tip position comparison.

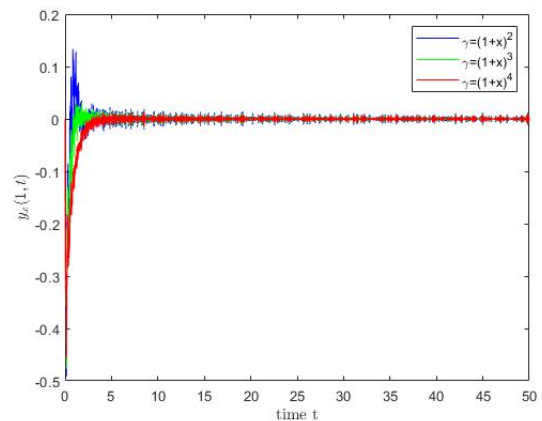


Figure 16: Tip angle comparison.

It is found that as the value of γ increases, the oscillations of the beam tips are attenuated, leading to a rapid convergence to the steady state.

3.2.3. Study of the spectrum

Now, by implementing the spectrum matrix L , we represent the spectrum associated with the system for different values of γ . On the Figures 17, 18, and 19, we have represented a distribution of $4N$ eigenvalues for $\gamma(x) = (1 + x)^2$, $\gamma(x) = (1 + x)^3$, and $\gamma(x) = (1 + x)^4$, respectively. We observe that when $m = EI = 1$, the location of spectrum moves rapidly on the left-hand side of the complex plane.

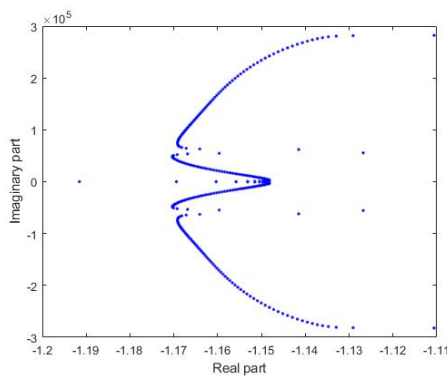


Figure 17: Representation of spectrum for $\gamma(x) = (1 + x)^2$.

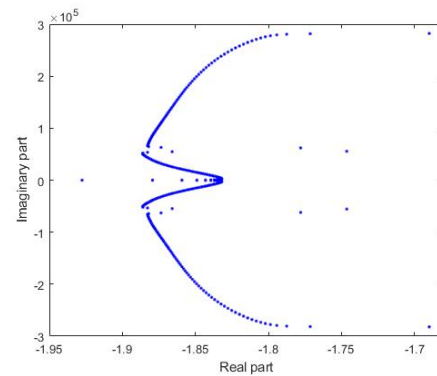


Figure 18: Representation of spectrum, when $\gamma(x) = (1 + x)^3$.

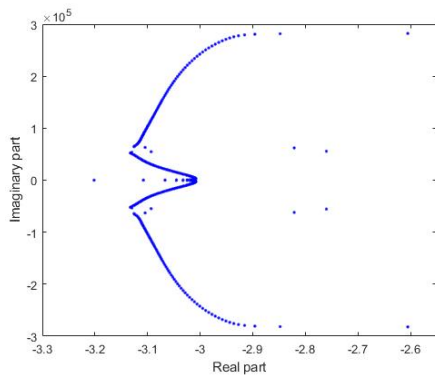


Figure 19: Representation of spectrum, when $\gamma(x) = (1 + x)^4$.

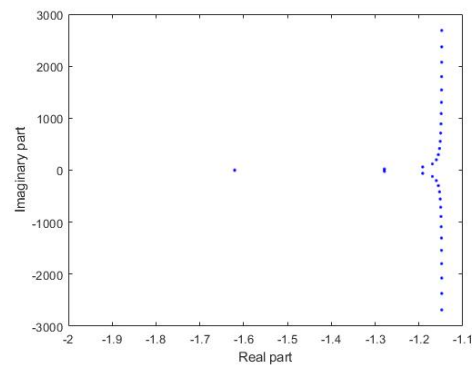


Figure 20: Asymptote of the spectrum for $\gamma(x) = (1 + x)^2$.

We notice a spectrum family whose real part is negative. This makes the system exponentially stable as long as $\gamma > 0$. We also illustrate the asymptote for uniform case, where we consider variable γ :

$$\lim_{n \rightarrow \infty} \operatorname{Re} \lambda_n = \frac{-1}{2h} \int_0^1 \gamma(x) dx.$$

Figures 20, 21, and 22 show the graphical representation of the asymptotes for different values of γ mentioned above. We can see the eigenvalue pairs λ_n of the system approach the imaginary axis as $n \rightarrow \infty$.

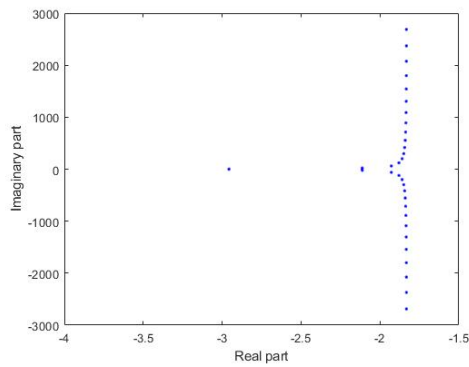


Figure 21: Asymptote of the spectrum for $\gamma = (1 + x)^3$.

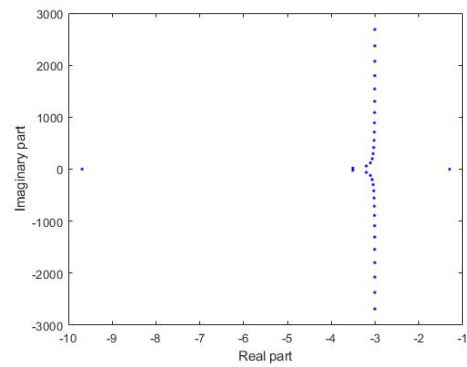


Figure 22: Asymptote of the spectrum for $\gamma = (1 + x)^4$.

3.3. Nonuniform case with constant damping γ

We choose $m(x) = (1 + x)^4$, $EI(x) = (1 + x)^2$. The simulations are performed for three different cases: a) $\gamma(x) = 5$; b) $\gamma(x) = 10$; and c) $\gamma(x) = 15$.

3.3.1. Representation of the deflection and energy

Figures 23, 24, and 25 represent the deflection of beam $y(x, t)$ for all three cases a), b), and c), respectively. The decay of energy function on the time interval $[0, 50]$ for cases a), b), and c) is shown in Figure 26.

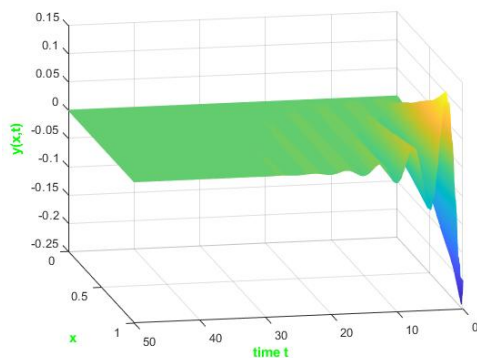


Figure 23: Displacement of the whole beam $y(x, t)$.

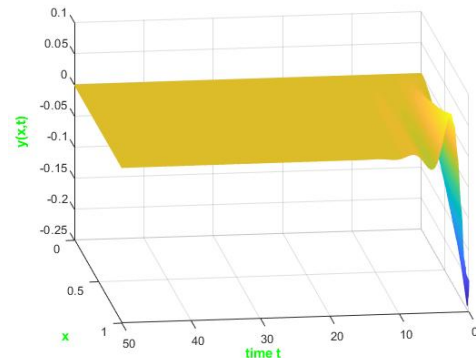


Figure 24: Displacement of the whole beam $y(x, t)$.

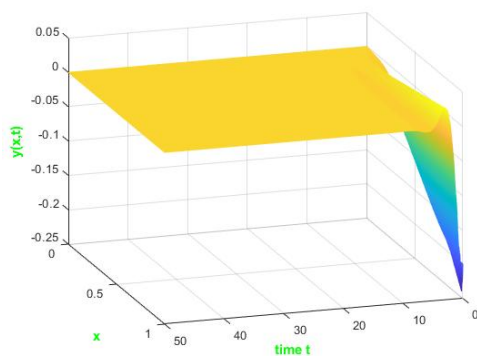


Figure 25: Displacement of the whole beam $y(x, t)$.

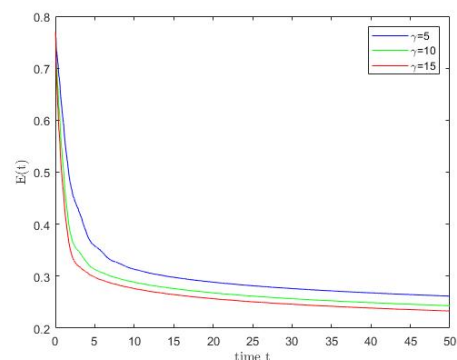


Figure 26: Influence of the damping γ on the energy.

3.3.2. Representation of tip position and tip angle

The comparison of the tip position $y(1; t)$ and the tip angle $y_x(1; t)$ for these three cases for the variable damping is illustrated in the Figures 27 and 28, for the time interval $[0, 50]$.

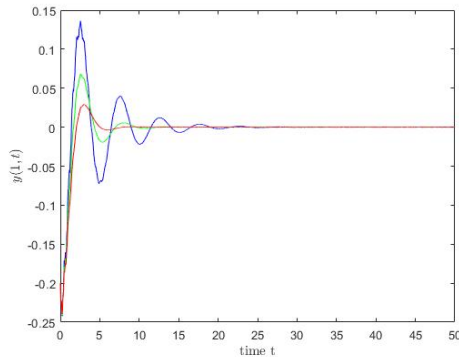


Figure 27: Displacement of the free end.

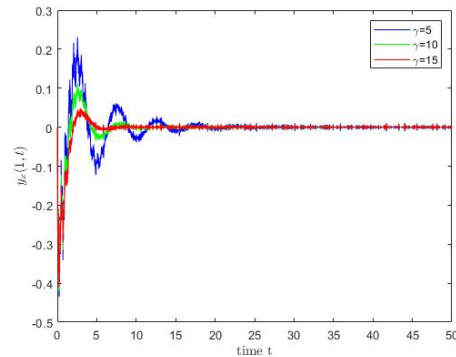


Figure 28: Tip angle comparison.

3.3.3. Study of the spectrum

On the Figures 29 and 30, we have represented a distribution of 4N eigenvalues for $\gamma = 5$ and $\gamma = 10$.

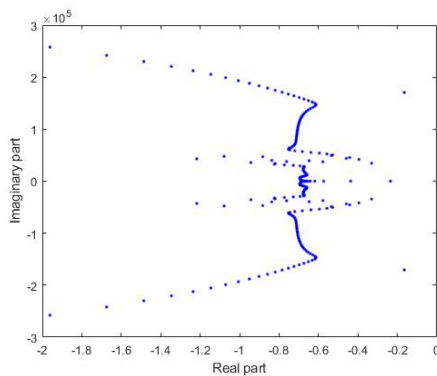


Figure 29: Representation of spectrum for $\gamma = 5$.

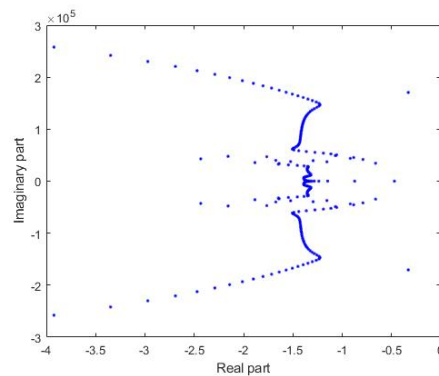


Figure 30: Representation of spectrum for $\gamma = 10$.

We notice a spectrum family whose real part is negative. This makes the system exponentially stable as long as $\gamma > 0$. We also observe a shift of the spectrum to the left.

Now, we also illustrate the asymptote for nonuniform case:

$$\lim_{n \rightarrow \infty} \operatorname{Re} \lambda_n = \frac{-1}{2h} \int_0^1 \left(\frac{\gamma(x)}{m(x)} \right) \left(\frac{m(x)}{EI(x)} \right)^{1/4} dx > 0.$$

First, we plot the spectrum for $\gamma = 5$ (Figure 31). We observe values to the right of the asymptote.

Figure 32 shows the representation of the spectrum for $\gamma = 10$. We observe values to the right of the asymptote.

3.4. Nonuniform case with variable damping γ

Let $m(x) = (1 + x)^4$, $EI(x) = (1 + x)^2$. The simulations are performed for three different cases: a) $\gamma(x) = (1 + x)^2$; b) $\gamma(x) = (1 + x)^3$; and c) $\gamma(x) = (1 + x)^4$.

The numerical results provided in this section verify the prediction of the convergence of the solution to the steady state $y \equiv 0$ and the non-increasing of energy $\mathbb{E}(t)$.

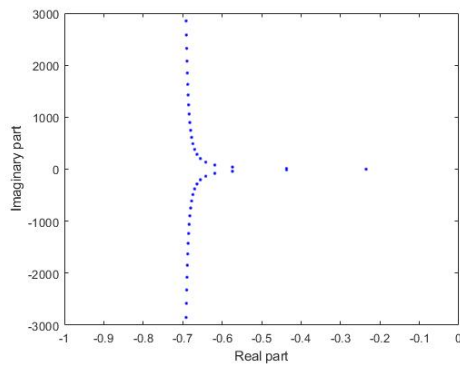


Figure 31: Asymptote of the spectrum for $\gamma = 5$.

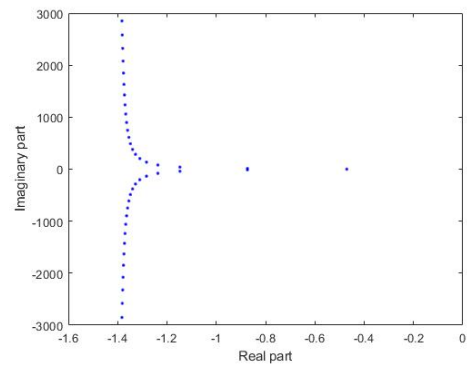


Figure 32: Asymptote of the spectrum for $\gamma = 10$.

3.4.1. Representation of the deflection and energy

Figures 33, 34, and 35 represent the deflection of beam $y(x, t)$ for all three cases a), b), and c), respectively. The decay of energy function on the time interval $[0, 50]$ for cases a), b), and c) is shown in Figure 36.

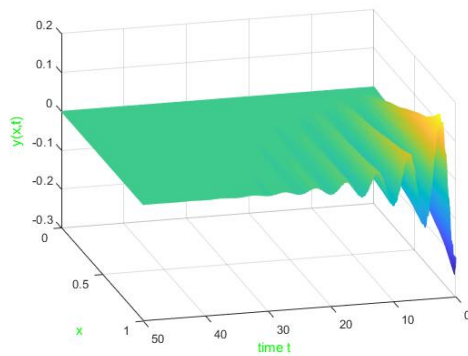


Figure 33: Deflection $y(x, t)$.

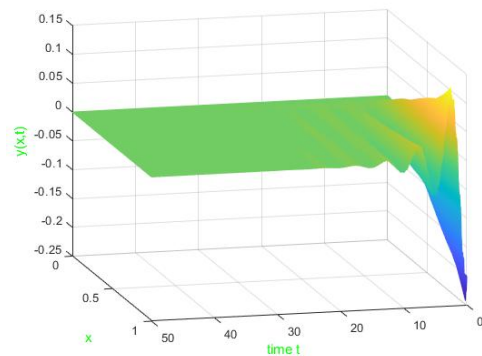


Figure 34: Deflection $y(x, t)$.

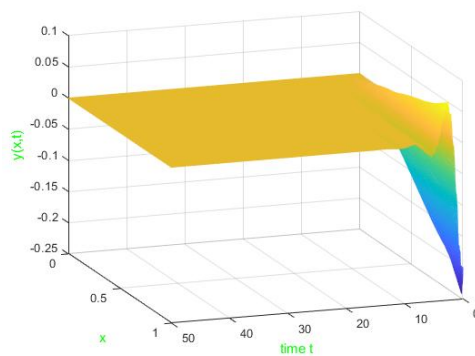


Figure 35: Deflection $y(x, t)$.

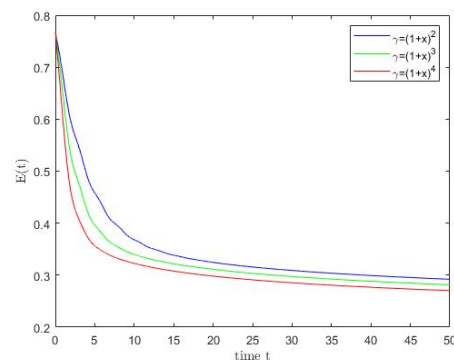


Figure 36: Influence of the damping γ on the energy.

3.4.2. Representation of tip position and tip angle

The comparison of the tip position $y(1; t)$ and the tip angle $y_x(1; t)$ for these three cases for the variable damping are illustrated in the Figures 37 and 38, for the time interval $[0, 50]$. It can be noticed that in the

variable case of damping resulted in a slower decay of the beam and suppressed the oscillations of the tip less quickly than in the constant case of damping.

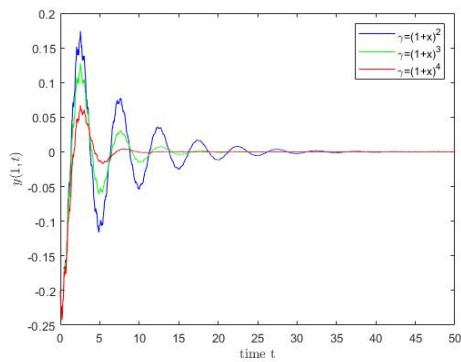


Figure 37: Tip position comparison.

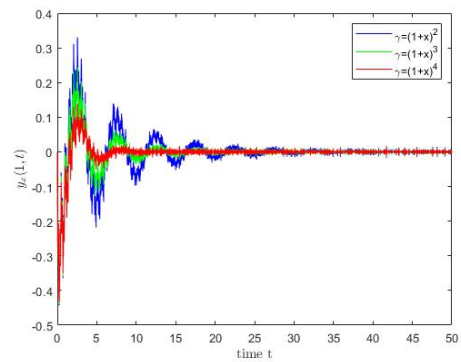


Figure 38: Tip angle comparison.

3.4.3. Study of the spectrum

On the Figures 39 and 40, we have represented a distribution of 4N eigenvalues for $\gamma(x) = (1 + x)^2$ and $\gamma(x) = (1 + x)^3$. We notice a spectrum family whose real part is negative. This makes the system

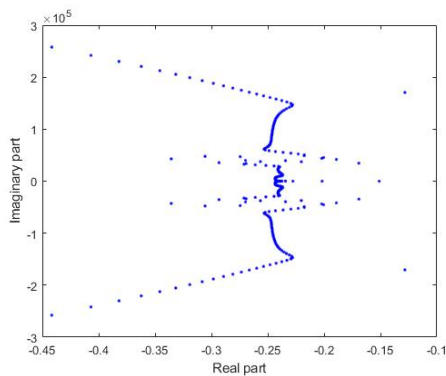


Figure 39: Representation of spectrum for $\gamma(x) = (1 + x)^2$.

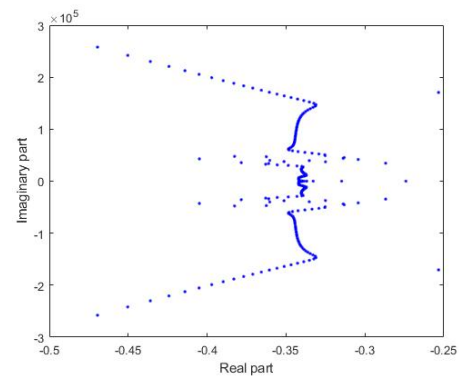


Figure 40: Representation of spectrum for $\gamma(x) = (1 + x)^3$.

exponentially stable as long as $\gamma > 0$. We also observe a shift of the spectrum to the left. Figure 41 shows us a spectrum which is certainly contained in the negative real part but whose appearance is totally different from the other two.

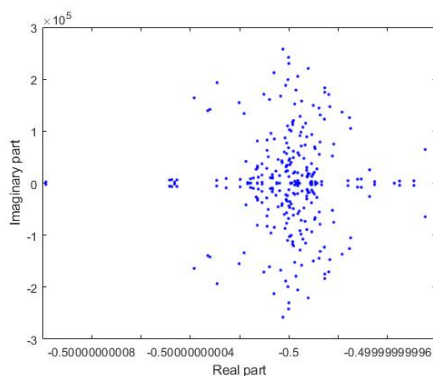


Figure 41: Representation of spectrum for $\gamma(x) = (1 + x)^4$.

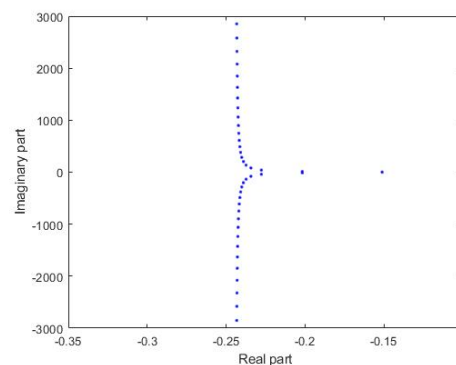


Figure 42: Asymptote of the spectrum for $\gamma(x) = (1 + x)^2$.

Now, we also illustrate the asymptote for nonuniform case:

$$\lim_{n \rightarrow \infty} \operatorname{Re} \lambda_n = \frac{-1}{2h} \int_0^1 \left(\frac{\gamma(x)}{m(x)} \right) \left(\frac{m(x)}{EI(x)} \right)^{1/4} dx > 0. \quad (3.1)$$

First, we plot the spectrum for $\gamma(x) = (1+x)^2$ (see Figure 42) and $\gamma(x) = (1+x)^3$ (see Figure 43). Values are seen in the area to the right of the asymptote.

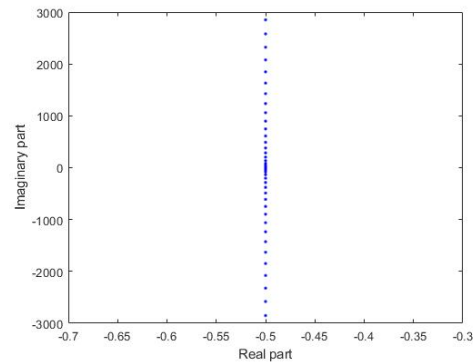
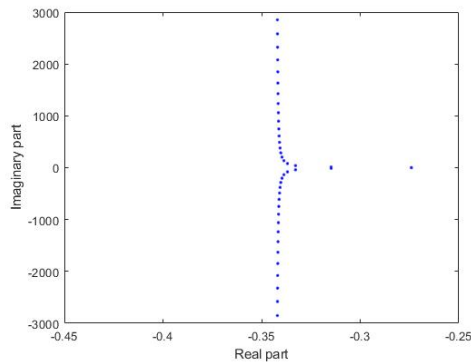


Figure 43: Asymptote of the spectrum for $\gamma(x) = (1+x)^3$.

Figure 44: Asymptote of the spectrum for $\gamma(x) = (1+x)^4$.

Finally, we represent the asymptote for $\gamma(x) = (1+x)^4$. We observe no point to the left of it. It is important to note in this case that the value of the abscissa of the asymptote is the same as that found for $\gamma = 1$. This is justified by the choice of the parameters $EI(x)$, $m(x)$, and $\gamma(x)$. We can see that with these values a simplification of the expressions occurs in (3.1). This leads to the case where $\gamma = 1$, hence the observation of scattered eigenvalues as in Figure 7.

4. Conclusion

In this article, a damped Euler-Bernoulli beams that have nonuniform thickness or density is developed. From all of the above observations, we assert that varying the damping control γ has a huge influence. It improves the energy decay rate of the system. Because we see that the more increase the value of γ , the more the spectrum moves to the left. In [17], the author theoretically proved that the positive value of damping was sufficient to establish the exponential stability of the system. This is consistent with our numerical results. Moreover, we illustrated the asymptote and found that the optimal energy decay rate is in general determined by the low frequency eigenvalues, those on the right side of the asymptote. Thus, the numerical method implemented, through its finesse, allowed us to appreciate the impact of the rotation control on the energy decay rate of the system studied. This is not practically visible at the theoretical level.

Acknowledgements

The authors are very grateful to one of the referees for their comments and suggestions.

References

- [1] H. T. Banks, I. G. Rosen, *Computational methods for the identification of spatially varying stiffness and damping in beams*, *Control Theory Adv. Tech.*, **3** (1987), 1–32. 2.2
- [2] G. J. M. Bomisso, K. A. Touré, G. Yoro, *A study of exponential stability for a flexible Euler-Bernoulli beam with variable coefficients under a force control in rotation and velocity rotation*, *Glob. J. Pure Appl. Math.*, **13** (2017), 6991–7008. 1

- [3] G. J. M. Bomisso, A. Touré, G. Yoro, *Stabilization of variable coefficients Euler-Bernoulli beam with viscous damping under a force control in rotation and velocity rotation*, J. Math. Res., **9** (2017), 1–13. 1
- [4] S. C. Brenner, L. R. Scott, *The mathematical theory of finite element methods*, Springer, New York, (2008). 2.3.2
- [5] S. M. Choo, S. K. Chung, R. Kannan, *Finite element Galerkin solutions for the strongly damped extensible beam equations*, Korean J. Comput. Appl. Math., **9** (2002), 27–43. 2.3.2, 2.3.2
- [6] P. G. Ciarlet, *The Finite Element Method for Elliptic problems*, North-Holland Publishing Co., Amsterdam-New York-Oxford, (1978). 1
- [7] G. H. Golub, C. F. Van Loan, *Matrix computations*, Johns Hopkins University Press, Baltimore, MD, (1989). 1
- [8] K. A. A. Hermith, C. Adama, Coulibaly, T. K. Augustin, *Numerical approximation of spectrum for variable coefficients Euler-Bernoulli beams under a force control in position and velocity*, Int. J. Appl. Math., **30** (2017), 211–228. 1
- [9] C. B. Moler, G. W. Stewart, *An algorithm for generalized matrix eigenvalue problems*, SIAM J. Numer. Anal., **10** (1973), 241–256. 1
- [10] M. E. Patrice, T. K. Augustin, T. M. Mathurin, *Numerical approximation of the spectrum for a hyperbolic equation with boundary condition*, Far East J. Appl. Math., **60** (2011), 41–53. 1
- [11] M. A. Ragusa, A. Tachikawa, *Boundary regularity of minimizers of $p(x)$ -energy functionals*, Ann. Inst. H. Poincaré C Anal. Non Linéaire., **33** (2016), 451–476. 1
- [12] J. Rappaz, M. Picasso, *Introduction à l'analyse numérique*, Presses Polytechniques et Universitaires Romandes, Lausanne, (1998). 1
- [13] A. Scapellato, *Regularity of solutions to elliptic equations on Herz spaces with variable exponents*, Bound. Value Probl., **2019** (2019), 9 pages. 1
- [14] G. Strang, G. J. Fix, *An analysis of the finite element method*, Prentice-Hall, Inc., Englewood Cliffs, N.J., **1973** (1973), 154 pages. 2.4.2
- [15] K. A. Touré, A. Coulibaly, A. A. H. Kouassi, *Riesz basis and exponential stability for Euler-Bernoulli beams with variable coefficients and indefinite damping under a force control in position and velocity*, Electron. J. Differ. Equ., **2015** (2015), 1–20. 1
- [16] T. S. Wang, *A Hermite cubic immersed finite element space for beam design problems*, Thesis, Blacksburg, Virginia, (2005). 2.3.1
- [17] J.-M. Wang, G.-Q. Xu, S.-P. Yung, *Riesz basis property, exponential stability of variable coefficient Euler-Bernoulli beams with indefinite damping*, IMA J. Appl. Math., **70** (2005), 459–477. 1, 1, 1, 2.1, 4